NEAR FIELD UWB LCMV IMAGING FOR BREAST CANCER DETECTION WITH ENTROPY BASED ARTIFACTS REMOVAL

Wanjun Zhi, Francois Chin and Michael Chia

Institute for Infocomm Research, Singapore

ABSTRACT

In this paper, we propose a near field wideband linear constraint minimum variance (LCMV) beamforming with entropy based artifacts removal for UWB imaging in breast cancer detection. We define an entropy function in antenna domain to measure the similarity of the different antenna signals and design a window function to eliminate the very similar artifacts at all antennas. This algorithm requires no prior knowledge about the breast and tumor, and brings no distortion to the tumor reflection.

After removing the artifacts, we model the tumor as a near field region source. By applying the coherent signal subspace method, a wideband near field LCMV beamforming to the region source is developed. The output power of the beamforming forms the image of the breast with tumor embedded. Applied to 2D computed finite-difference time-domain (FDTD) data, the algorithm clearly identifies the 2mm-diameter tumor. Simulation results also demonstrate the efficiency and robustness of the proposed algorithm.

1. INTRODUCTION

Microwave imaging is being investigated for breast cancer detection due to its advantages over the primarily used X-ray mammography, such as non-ionizing, noninvasive, low power, high image quality, and unnecessary breast compression [1]. UWB radar technique, which is analogous to the ground penetrating radar, is extensively studied [2-6]. The UWB pulse is emitted by a small antenna, which then picks up the returning wave after it has been reflected by the breast. With the significant contrast in dielectric properties of normal and malignant breast tissues, tumors give larger reflection than regular breast tissue. By scanning the microwaves over the breast, the reflections can be added up to make an image of the tumor.

One method employs simple delay-and-sum beamforming [2-4] to form an image of the breast scanned. As the it has limited resolution, the other method, microwave imaging via space-time (MIST) beamforming [5, 6], takes into account the frequency-dependent propagation of UWB signal, and uses space-time filter to implement the wideband beamforming. Simulation results show that the MIST beamforming offers significant improvements over delay-and-sum beamforming at the cost of computational requirements, as high-order filters are required due to the ultra wide bandwidth of the system.

These two methods consider the tumor as a point source, which is unnecessarily true in practice. In this paper we model the tumor as a region source, and locate the tumor with wideband linear constraint minimum variance (LCMV) beamforming.

The backscattered tumor signal is modeled as an ultra wideband near field signal. By applying the coherent signal subspace (CSS) method in [8] to the near filed beamforming, the wideband problem is transformed to a narrow band problem via a focusing matrix. The region source can be considered as several point sources, and we thus add the linear constraints to these point sources to control the beamforming response in the tumor region.

The proposed method in this paper is also different from the methods in [2-6] in artifact removal algorithm. Artifact removal is a kind of preprocessing to the received reflection waveforms, which removes the large magnitude skin-breast interface reflection so that the tumor reflection can be used for the cancer detection. [3] assumes the artifacts in the M antennas are identical, and simply subtracts the average of these M received signals from each antenna waveform. While [5] presents an algorithm based on space-time Wiener filtering under the assumption that the skin-breast artifact at each antenna is a filtered combination of the signal at all other antennas. The algorithm can efficiently remove the artifacts at the expense of an insignificant distortion in tumor reflection. It requires the prior knowledge of time duration in which only artifacts exist, and is also computationally complicated.

The proposed artifacts removal algorithm is based on the simple entropy computation. With no prior knowledge, it efficiently removes the artifacts with no distortion in tumor reflection. Observing that the artifacts at all the antennas are very similar, we define an antenna domain entropy function to measure the similarity of different antenna signals, and design a window function according to the similarity to eliminate the artifact.

2. PROBLEM FORMULATION AND ARTIFACTS REMOVAL

2.1. Received signal model

Similar to [3], the system employs an antenna placed at some specific positions (for instance, M positions) along the breast skin. Exciting the antenna at each position with a short pulse and picking the back scatter response at the same position will synthetically results in M received signals, which are considered to be the received signals of an active *M*-element array.

The received signal at the *i*th antenna $z_i(t)$ contains the incident signal $I(t)$, the response from skin-breast interface $b_i(t)$, and the reflection from tumor as well as other possible scattering objects $x_i(t)$,

$$z_i(t) = I(t) + b_i(t) + x_i(t), \qquad i = 1, \cdots, M . \tag{1}$$

$I(t)+b_i(t)$ is orders of magnitude larger than the tumor reflection, and it is the artifact to be removed from the received signal before performing tumor detection with $x_i(t)$.

Analyzing the M received signals, $[z_1(t),\cdots,z_M(t)]$, $I(t)$ are identical at all antennas, $[b_1(t),\cdots,b_M(t)]$ have high similarity, while $[x_1(t),\cdots,x_M(t)]$ are a series of delayed and attenuated pulses. $I(t)+b_i(t)$ appears earlier than $x_i(t)$ for shorter distance from the antenna to the skin than to the tumor. $I(t)+b_i(t)$ is also separated from $x_i(t)$ in time axis due to the resolution of very short pulse, thus by multiplying a window function to the received signal, we can get rid of the artifact in times that not included in the window.

2.2. Entropy based artifact removal algorithm

Entropy is a measure of variation, hence the entropy of the antenna signals at each time instant will describe the variation or similarity of the signals at that time. Similar artifacts in earlier time result in larger entropy and tumor reflections in later time result in lower entropy.

The α -th order Renyi entropy at time t is defined as:

$$H_\alpha(t)=\frac{1}{1-\alpha}\log\left\{\sum_{i=1}^{M}[p_i(t)]^\alpha\right\}, \tag{2}$$

where α is real positive, and $p_i(t)=\|z_i(t)\|^2\Big/\sum_{i=1}^{M}\|z_i(t)\|^2$.

Since our concern is the similarity of the pulses of different antenna in a certain time duration T, we use the moving average filter to smooth the entropy $H_\alpha(t)$ in the period of T. The smoothed entropy is

$$H_\alpha^s(t)=\frac{1}{T}\int^{t+T}H_\alpha(t)dt\ . \tag{3}$$

Time window function can be designed in several ways. To avoid distortion to the tumor reflection, we design a rectangular window in the following way.

Extending the definition of theoretical dimension in [7], we consider the theoretical dimension of signal $[z_1(t),\cdots,z_M(t)]$ to be $e^{H_\alpha^s(t)}$, which is a value between 1 and M describing how many of the M antenna signals are significant at time *t*. By comparing the dimension with some threshold N_0, the time window function can be designed as

$$W(t)=\begin{cases}0 & e^{H_\alpha^s(t)}>N_0\\ 1 & \text{otherwise}\end{cases}, \tag{4}$$

which has zero value at times when larger entropy occurs. The artifact removed signal is then written as

$$x_i(t)=W(t)z_i(t),\qquad i=1,\cdots,M\ . \tag{5}$$

3. WIDEBAND LCMV BEAMFORMING FOR TUMOR DETECTION

3.1. Near field mathematical model

After removing the artifact, the reflections from tumor and other scattering objects can be simplified as a near field model

$$x_i(t)=\alpha_i s(t-\tau_i)+n_i(t), \tag{6}$$

where $s(t)$ is the transmitted pulse, and $n_i(t)$ is the *i*th sensor noise as well as other backscattered signals; the parameters α_i,τ_i are determined by the distance from the tumor at $\boldsymbol{p}_0$ to the *i*th sensor at $\boldsymbol{q}_i$ and the propagation velocity v, $\alpha_i=\|\boldsymbol{p}_0\|^2/\|\boldsymbol{p}_0-\boldsymbol{q}_i\|^2$ and $\tau_i=2\big(\|\boldsymbol{p}_0-\boldsymbol{q}_i\|-\|\boldsymbol{p}_0\|\big)/v$.

The corresponding frequency domain model is

$$\begin{aligned}X_i(\omega)&=\alpha_i e^{-j\omega\tau_i}S(\omega)+N_i(\omega)\\&=\frac{\|\boldsymbol{p}_0\|^2}{\|\boldsymbol{p}_0-\boldsymbol{q}_i\|^2}e^{-j2\omega(\|\boldsymbol{p}_0-\boldsymbol{q}_i\|-\|\boldsymbol{p}_0\|)/v}S(\omega)+N_i(\omega)\end{aligned}. \tag{7}$$

Writing the M received signals in vector form,

$$\boldsymbol{X}(\omega)=\boldsymbol{a}(\boldsymbol{p}_0,\omega)S(\omega)+\boldsymbol{N}(\omega), \tag{8}$$

where $\boldsymbol{a}(\boldsymbol{p}_0,\omega)$ is the steering vector,

$$\boldsymbol{a}(\boldsymbol{p}_0,\omega)=\|\boldsymbol{p}_0\|^2 e^{j2\omega\|\boldsymbol{p}_0\|/v}\left[\frac{e^{-j2\omega\|\boldsymbol{p}_0-\boldsymbol{q}_1\|/v}}{\|\boldsymbol{p}_0-\boldsymbol{q}_1\|^2}\cdots\frac{e^{-j2\omega\|\boldsymbol{p}_0-\boldsymbol{q}_M\|/v}}{\|\boldsymbol{p}_0-\boldsymbol{q}_M\|^2}\right]^{\mathrm{T}}. \tag{9}$$

The cross spectral density matrix used in the array processing is

$$\begin{aligned}\boldsymbol{R}_x(\omega)&=\mathrm{E}\left[\boldsymbol{X}(\omega)\boldsymbol{X}^{\mathrm{H}}(\omega)\right]\\&=\boldsymbol{a}(\boldsymbol{p}_0,\omega)\boldsymbol{R}_s(\omega)\boldsymbol{a}^{\mathrm{H}}(\boldsymbol{p}_0,\omega)+\boldsymbol{R}_n(\omega)\end{aligned}, \tag{10}$$

where $\boldsymbol{R}_s(\omega)=\boldsymbol{S}(\omega)\boldsymbol{S}^{\mathrm{H}}(\omega)$, and $\boldsymbol{R}_n(\omega)=\boldsymbol{N}(\omega)\boldsymbol{N}^{\mathrm{H}}(\omega)$.

3.2. Near field LCMV beamforming for region source

LCMV beamformer in [9] tries to minimize the output power subject to some constraints. That is, in frequency domain,

$$\min_{\boldsymbol{w}}\left[\boldsymbol{w}(\omega)^{\mathrm{H}}\boldsymbol{R}_x(\omega)\boldsymbol{w}(\omega)\right]\ \text{, s.t. }\boldsymbol{w}(\omega)^{\mathrm{H}}\boldsymbol{C}(\boldsymbol{p},\omega)=\boldsymbol{g}\ . \tag{11}$$

where $\boldsymbol{C}(\boldsymbol{p},\omega)$ is defined as a $M\times L$ -dimensional matrix, and $\boldsymbol{w}(\omega)^{\mathrm{H}}\boldsymbol{C}(\boldsymbol{p},\omega)=\boldsymbol{g}$ defines a set of L linear constraint equations controlling the beamformer response.

As tumor is not necessarily a point source, we consider the tumor to be a region source which includes several point sources around the focal point $\boldsymbol{p}_0$. Let $\boldsymbol{C}(\boldsymbol{p},\omega)=[\boldsymbol{a}(\boldsymbol{p}_1,\omega),\cdots,\boldsymbol{a}(\boldsymbol{p}_L,\omega)]$, with $\boldsymbol{p}_1,\cdots,\boldsymbol{p}_L$ being the position vectors in a small region around $\boldsymbol{p}$, and $\boldsymbol{g}=[1,\cdots,1]$, to guarantee the response in a region.

The optimal weight vector of (11) is

$$\boldsymbol{w}(\omega)=\boldsymbol{R}_x^{-1}(\omega)\boldsymbol{C}(\boldsymbol{p},\omega)\left[\boldsymbol{C}^{\mathrm{H}}(\boldsymbol{p},\omega)\boldsymbol{R}_x^{-1}(\omega)\boldsymbol{C}(\boldsymbol{p},\omega)\right]^{-1}\boldsymbol{g}\ , \tag{12}$$

and the output power of the beamformer is

$$P(\boldsymbol{p})=\int_\omega \boldsymbol{w}^{\mathrm{H}}(\omega)\boldsymbol{R}_x(\omega)\boldsymbol{w}(\omega)d\omega\ . \tag{13}$$

$P(\boldsymbol{p})$ forms the image of the breast tissue. The tumor is esitmated at $\hat{\boldsymbol{p}}_0$, which maximize the output power $P(\boldsymbol{p})$,

$$\hat{\boldsymbol{p}}_0=\max_{\boldsymbol{p}}[P(\boldsymbol{p})]\ . \tag{14}$$

Note that the optimal sensor weights are frequency dependent, and the output power is the incoherent combination of output power in the whole frequency band.

3.3. Wideband near field LCMV beamforming for region source

Coherent signal-subspace (CSS) method proposed for far field direction finding in [8] applies focusing matrix to transform the signal subspaces at different frequency bands to a reference frequency band, and coherently combines the signal subspaces in

the frequency band of interest. Coherently combining the wideband information provides advantages such as lower computational complexity and performance improvement. We extend this CSS method to the near field LCMV beamforming.

Given transform matrix $\boldsymbol{T}(\omega)$ satisfying

$$\boldsymbol{T}(\omega)\boldsymbol{a}(\boldsymbol{p}_0,\omega)=\boldsymbol{a}(\boldsymbol{p}_0,\omega_0), \tag{15}$$

where ω_0 is the reference frequency, we have the transformed signal

$$\boldsymbol{Y}(\omega)=\boldsymbol{T}(\omega)\boldsymbol{X}(\omega)=\boldsymbol{a}(\boldsymbol{p}_0,\omega_0)\boldsymbol{S}(\omega)+\boldsymbol{T}(\omega)\boldsymbol{N}(\omega). \tag{16}$$

The cross spectral density matrix becomes

$$\boldsymbol{R}_y(\omega)=\boldsymbol{a}(\boldsymbol{p}_0,\omega_0)\boldsymbol{R}_s(\omega)\boldsymbol{a}^{\mathrm{H}}(\boldsymbol{p}_0,\omega_0)+\boldsymbol{T}(\omega)\boldsymbol{R}_n(\omega)\boldsymbol{T}^{\mathrm{H}}(\omega), \tag{17}$$

and the combined cross spectral density matrix is obtained

$$\begin{aligned}\overline{\boldsymbol{R}}_y &= \int_{\omega}\boldsymbol{R}_y(\omega)d\omega \\ &=\boldsymbol{a}(\boldsymbol{p}_0,\omega_0)\left[\int_{\omega}\boldsymbol{R}_s(\omega)d\omega\right]\boldsymbol{a}^{\mathrm{H}}(\boldsymbol{p}_0,\omega_0)+\int_{\omega}\boldsymbol{T}(\omega)\boldsymbol{R}_n(\omega)\boldsymbol{T}^{\mathrm{H}}(\omega)d\omega. \\ &=\boldsymbol{a}(\boldsymbol{p}_0,\omega_0)\overline{\boldsymbol{R}}_s\boldsymbol{a}^{\mathrm{H}}(\boldsymbol{p}_0,\omega_0)+\overline{\boldsymbol{R}}_n\end{aligned} \tag{18}$$

LCMV beamforming for the transformed signal becomes

$$\min_{\boldsymbol{w}}\left[\boldsymbol{w}^{\mathrm{H}}\overline{\boldsymbol{R}}_y\boldsymbol{w}\right], \text{ s.t. } \boldsymbol{w}^{\mathrm{H}}\boldsymbol{C}(\boldsymbol{p},\omega_0)=\boldsymbol{g}. \tag{19}$$

The frequency independent optimal vector is

$$\boldsymbol{w}=\overline{\boldsymbol{R}}_y^{-1}\boldsymbol{C}(\boldsymbol{p},\omega_0)\left[\boldsymbol{C}^{\mathrm{H}}(\boldsymbol{p},\omega_0)\overline{\boldsymbol{R}}_y^{-1}\boldsymbol{C}(\boldsymbol{p},\omega_0)\right]^{-1}\boldsymbol{g}, \tag{20}$$

thereafter, the output power of beamforming is

$$P(\boldsymbol{p})=\boldsymbol{w}^{\mathrm{H}}\overline{\boldsymbol{R}}_y\boldsymbol{w}, \tag{21}$$

and the tumor location is estimated at $\hat{\boldsymbol{p}}_0=\max_{\boldsymbol{p}}[P(\boldsymbol{p})]$.

4. SIMULATION RESULTS

We apply the new method to the FDTD backscattered signals to demonstrate its effectiveness.

4.1 FDTD data acquisition

The computational electromagnetic model of the normal breast tissue is as described in [5], where the Debye model is adopted to account for the frequency dependence of the dielectric constant, ε_r, and the conductivity, σ, over the frequency band of interest (100 MHz to 20 GHz),

$$\varepsilon_r - j\frac{\sigma}{\omega\varepsilon_0}=\varepsilon_\infty+\frac{\varepsilon_s-\varepsilon_\infty}{1+j\omega\tau}-j\frac{\sigma_s}{\omega\varepsilon_0}. \tag{22}$$

The FDTD data are computed from the breast model in Fig.1, where 1-mm-thickness skin and a 2mm-diameter tumor centered at (7.55, 6.55) are included. In the FDTD computation, the spatial grid resolution is 0.5mm, and the time step is 0.866ps. The black dots mark 13 antenna positions. A 110-ps (128 time steps) differentiate Gaussian pulse is transmitted and recorded at one position each time. A subset of received signals is plotted in Fig.2. The left column shows the data in earlier time, which are the large magnitude artifacts, and the right column shows the data in later time, which are the weak reflections from the normal tissue and tumor.

4.2. Entropy-based artifacts removal

We sample the FDTD data with sampling period 17.33ps (57.7GHz sampling frequency). In the artifacts removal algorithm, $\alpha=3$ is chosen. The 3rd Renyi entropy at each sampling instant and the smoothed entropy are shown in Fig. 3. It is obvious that the very similar portions of the received data in earlier time give large entropy. The theoretical dimension and the rectangular window are illustrated in Fig. 4, where the threshold is set to be $N_0=6$, approximately half of the antenna number. The artifacts are easily removed by multiplying the rectangular window to the received data.

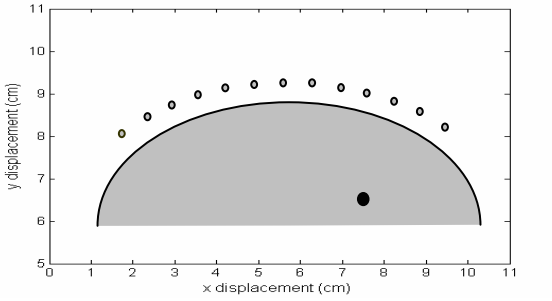

Fig.1. 2D breast model to compute FDTD data

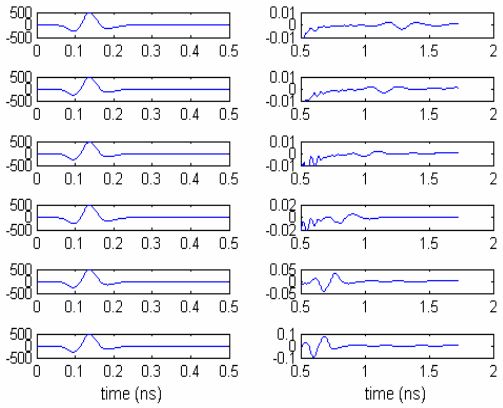

Fig. 2. The received signal at antenna position #2, 4, 6, 8, 10, 12: the left column is the received signal in earlier time (artifact), the right column is the received signal in later time (mainly caused by tumor reflection)

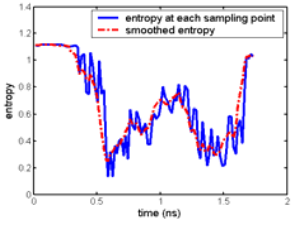

Fig.3 The entropy as a function of time

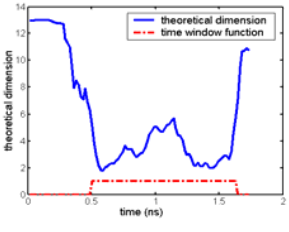

Fig.4 The theoretical dimension and time window function

4.3. Wideband LCMV beamforming for tumor detection

The results of applying the wideband LCMV beamforming to the artifact removed signal are shown in Fig. 5. Fig. 5(a) is the color

image of the breast by the use of beamforming output power. The output power focus in the tumor region. Although the peak power occurs at (7.45, 6.55) which deviates from the center point of the true location of the tumor (7.55, 6.55), the contours in Fig. 5(b) show that the -10dB region contains the dotted circle, representing the true tumor region.

In the LCMV beamforming, we assume a simple near field propagation model with frequency independent velocity in the breast tissue (also frequency independent dielectric constant ε_r, since $v = c/\sqrt{\varepsilon_r}$), while the simulation data is acquired by the frequency dependent model in (22). To investigate the robustness of the LCMV beamforming, we assume that ε_r used in beamforming mismatch that used in the FDTD simulation. Table I gives the location of the peak power in 4 scenarios with different dielectric constant assumed in beamforming. The tumor can be detected in all cases, although the estimated peak power point has a bias due to the difference between actual and assumed dielectric constant.

We note that even when the assumed dielectric constant is equal to the actual dielectric constant in FDTD simulation, there still exists a bias. One reason is that the frequency independent velocity used in near field model, and the other is that, two propagation medium, free space and breast tissue, are involved the data acquisition system due to the antenna being set in free space, but the propagation difference is ignored in beamforming.

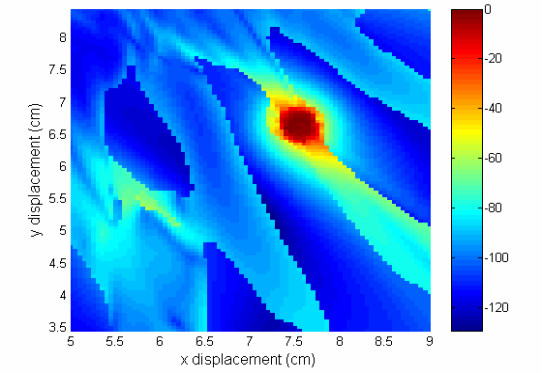

Fig.5 (a). Color image of LCMV beamforming output for breast with tumor embedded

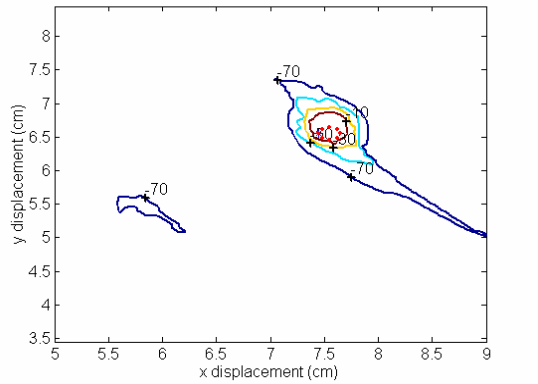

Fig.5 (b). Output power contours of the wideband LCMV beamforming

Table I. Estimated tumor location when dielectric constant assumed mismatch that used in data acquisition

Dielectric constant applied in FDTD data acquisition at 6GHz: $\varepsilon_r = 9.8$				
Assumed in beamforming at 6GHz	$\varepsilon_r = 4.9$	$\varepsilon_r = 9.8$	$\varepsilon_r = 15.7$	$\varepsilon_r = 21.5$
Estimated location $\hat{\boldsymbol{p}}_0$	(7.60,6.65)	(7.45,6.55)	(7.55,6.70)	(7.55,6.75)

5. CONCLUSIONS

This paper proposes a near field wideband LCMV beamforming with entropy based artifacts removal for UWB imaging in breast cancer detection. This artifacts removal algorithm requires no prior knowledge about the breast, and brings no distortion of the tumor reflection. It is not only simple to use, but efficient.

The wideband near field LCMV beamforming to region source successfully detects the 2mm-diameter tumor with the simulated 2D FDTD data of a homogeneous breast model. Small tumor can be detected even in the scenarios that the breast tissue dielectric constant assumed in beamforming mismatches that used in actual FDTD data acquisition, which demonstrate the efficiency and robustness of new algorithm.

6. REFERENCES

[1] E. C. Fear, P. M. Meaney & M. A. Stuchly, "Microwaves for breast cancer detection*?", IEEE potentials*, 2003

[2] E. C. Fear and M. A. Stuchly, "Microwave detection of breast cancer," *IEEE Trans. Microwave Theory Tech.*, vol. 48, no. 11, pp. 1854–1863, Nov. 2000.

[3] Xu Li; Hagness, S.C., "A confocal microwave imaging algorithm for breast cancer detection," *IEEE Microwave and Wireless Components Letters*, vol. 11, pp.130– 132, Mar. 2001.

[4] E. C. Fear, X. Li, S. C. Hagness, and M. Stuchly, "Confocal microwave imaging for breast cancer detection: Localization of tumors in three dimensions," *IEEE Trans. Biomed. Eng.*, vol. 49, no. 8, pp. 812–822, Aug. 2002.

[5] E. J. Bond, X. Li, S. C. Hagness, and B. D. Van Veen, "Microwave imaging via space–time beamforming for early detection of breast cancer," *IEEE Trans. Antennas Propagat.*, vol. 51, pp. 1690–1705, Aug. 2003.

[6] X. Li, S. K. Davis, S. C. Hagness, D. W. van der Weide, and B. D. Van Veen, "Microwave imaging via space-time beamforming: Experimental investigation of tumor detection in multilayer breast phantoms," *IEEE Trans. Microwave Theory Tech.*, vol. 52, no. 8, pp. 1856–1865, Aug. 2004.

[7] Coifman, R. R. and Wickerhauser, M.V., "Entropy-based algorithms for best basis selection," *IEEE Trans. Information Theory*, vol. 38, pp. 713 - 718, Mar. 1992.

[8] Wang, H., and Kaveh, M., 'Coherent signal-subspace processing for the detection and estimation of angles of arrival of multiple wide-band sources', *IEEE Trans. Acoust. Speech Signal Process.*, vol. 33, pp. 823–831, 1985,

[9] Van Trees, H.L., *Detection, estimation, and modulation theory: Part IV,* Wiley Interscience, New York, 2002